

Accelerometer-based Orientation Sensing for Head Tracking in AR & Robotics

Matthew S. Keir^{1,2}, Chris E. Hann¹, J. Geoffrey Chase¹, and XiaoQi Chen¹

¹Department of Mechanical Engineering,

²Human Interface Technology Lab NZ,

University of Canterbury, Christchurch, New Zealand

matthew.keir@hitlabnz.org

Abstract

This work seeks to improve dynamic accuracy of viewpoint tracking for Augmented Reality. Using an inverted pendulum to model the head, dynamic orientation sensing for a single degree of rotation in a vertical plane is achieved using only a dual axis accelerometer. A unique solution is presented as conventional approaches to solve the model equations fail to produce stable results due to ill conditioning. Accuracy is limited by the noise and model error. However, dynamic tracking with better than 1° accuracy is achieved analytically and experimentally, proving the concept.

Keywords: head tracking, head motion model, inverted pendulum, orientation sensing, accelerometers

1 Introduction

Augmented Reality (AR) systems using head mounted displays (HMDs) require position and orientation (pose) information of the users viewpoint to overlay computer imagery correctly. Tracking accuracy and system latency are crucial to providing a compelling and useful AR application. Robust tracking systems are available for quasi-static applications. However, when applied in more dynamic applications they fail to produce the accuracy required.

Many different technologies have been applied to the head tracking problem, although no one technology tracks well for all applications [1]. As a result hybrid approaches have been taken ([2], [3], [4]) to improve accuracy and robustness by utilising two or more complementary technologies. Inertial tracking is often included in such approaches.

The inertial measurement units (IMUs) used for head tracking usually contain micro-electro-mechanical systems (MEMS). Specifically, rate gyroscopes (gyros) and accelerometers. High update rates and small size reduces system latency and allows unobtrusive packaging. However, measurements from these accelerometers and gyros require integration to obtain position and orientation. Numerical integration of noisy signals causes the results to drift. For the gyro this drift requires correction. However with the accelerometer drift corrupts the position measurement entirely due to the double integration required. Hence, inertial devices are only useful for tracking orientation in this application. Importantly AR systems are more sensitive to orientation error than position error, as the orientation error is scaled by the distance to the viewed object [5].

Accelerometers sense dynamic accelerations and also the acceleration due to gravity. As a result accelerometers can be very useful in tilt or orientation applications. For a stationary object determining

the orientation with respect to gravity is a trivial problem. However, when other motion is introduced the acceleration signal is modified by the dynamic accelerations, leading to orientation errors.

One approach to this problem is to take advantage of the burst like nature of head motion and correct for gyro drift during natural pauses [6]. However [7], shows orientation is improved using accelerometers to aid the gyroscope during human kinematic measurement, but does not detail the motion. Thus a full solution using only one sensor is lacking.

Commercial IMUs suitable for tracking 3DOF head motion include, the InertiaCube3 [8], 3d-Bird [9], MTx [10] and the 3DM-DH [11]. These IMUs typically contain three rate gyros, accelerometers and magnetometers. However, these devices are not optimised for individual applications although some allow the user to define initial filtering. None are yet fully proven in a highly dynamic environment.

Head motion for most applications is well below 2 Hz [12]. However, applications such as outdoor gaming demand much higher dynamic performance. Most approaches to improving dynamic tracking involve using Kalman filtering to fuse data from different sources and provide prediction to reduce system latency [13], [14]. The Kalman filter uses a model of the motion to predict for the next iteration step, this is not feasible with an unstable or unknown head motion model.

This paper seeks to improve inertial sensing for pitch and roll in a highly dynamic environment using minimal numbers of low cost sensors. Using an inverted pendulum to model the head, it is shown that dynamic orientation sensing can be achieved using only accelerometers. The results offer some potentially unique outcomes in application spaces such as robotics and manufacturing, and head motion sensing for AR.

2 METHOD

2.1 Model – Rotation in a Vertical Plane

An inverted pendulum is used to model the head with a dual axis accelerometer positioned along the pendulum, in the plane of rotation. The radius of rotation for the head may be a function of the degree of rotation. However, for this proof of concept the radius is considered to be fixed.

Figure 1 shows the components of acceleration applied to a particle at radius R for in-plane rotation (θ) of the head or pendulum. These tangential, centripetal and gravitational (g) accelerations and are sensed by the accelerometer axes A_y and A_x . The accelerometer is positioned at a fixed angle λ to the tangent of rotation, where $\lambda = \pi/4$ provides optimal sensitivity to gravity on both accelerometer axes. It also ensures the other accelerations are sensed by both axes which is useful to abate noise.

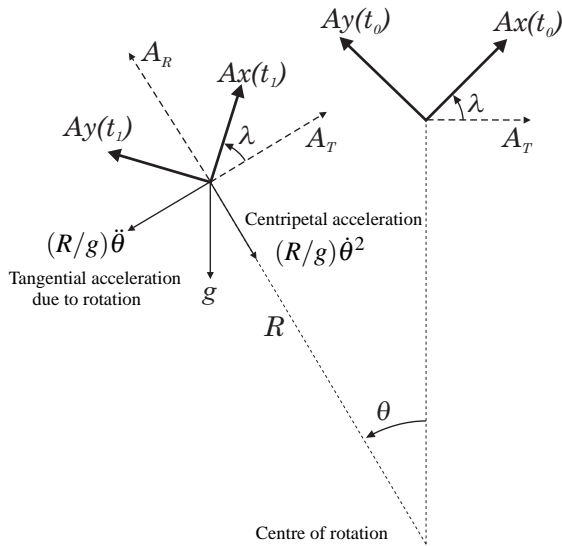


Figure 1: Acceleration vector diagram for a point at the end of an inverted pendulum, length R , undergoing a rotation of θ

The tangential ($A_T(t)$) and radial ($A_R(t)$) accelerations are derived from the measured accelerations below. Note that all accelerations and rotations ($\theta(t)$) are functions of time and that the “(t)” is dropped for clarity.

$$A_T = A_x \cos(\lambda) - A_y \sin(\lambda), \quad (1)$$

$$A_R = A_x \sin(\lambda) + A_y \cos(\lambda). \quad (2)$$

The accelerometer senses the acceleration of its proof mass relative to its casing. Hence, dynamic accelerations contribute in the opposite direction to that shown in figure 1. Resolving acceleration in terms of g along the tangential and radial axes provides two

independent ordinary differential equations (ODEs) for A_T and A_R :

$$A_T = (R/g)\ddot{\theta} - \sin(\theta), \quad (3)$$

$$A_R = (R/g)\dot{\theta}^2 - \cos(\theta). \quad (4)$$

It is important to note that these are not equations of motion, and are thus independent from any inertia, actuation force, damping or physiological limits that may influence the motion. The effect of any such terms will directly contribute the measured acceleration and is therefore captured by this model. This approach frees the problem from complex calibration or system identification procedures.

2.2 A General Engineering Approach

Solving equations (3) or (4), should provide the solution for θ . As a first attempt, data is generated for θ from a modified sine wave. The tangential acceleration is determined by substituting θ into equation (3). This ODE was solved in Maple using the default initial value problem (IVP) solver, a Fehlberg fourth-fifth order Runge-Kutta method, and in Matlab using a similar solver. Both Maple and Matlab failed to produce a stable solution.

Providing the solver with the actual initial conditions, $\theta(0)$ and $\dot{\theta}(0)$, results in the solution tracking the true solution for only two cycles before diverging. This result represents the pendulum spinning in the real system. Figure 2 shows that with a very low amplitude for θ the solution almost stabilises at π . Similar quasi-stability can be found at $-\pi$ when the pendulum is no longer inverted, a stable solution for the real pendulum. Including a damping term in the ODE can stabilise this solution. However, it proves to be of no use in determining the true rotation.

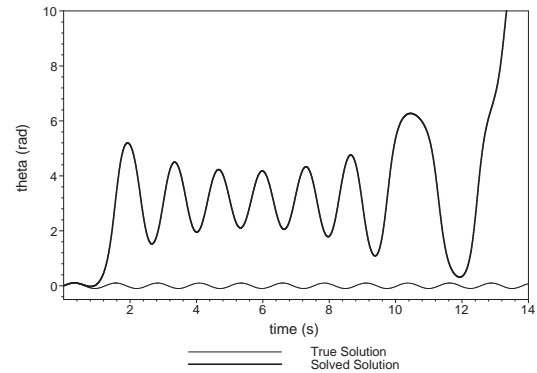


Figure 2: Simulated data, solved numerically. Note that the solved solution oscillates around π before blowing up completely

A second attempt combines the Equations, (3) and (4). Solving simultaneously also fails to produce a stable result. To gain a better understanding of the instability of the model and enable an analytical solution Equation (3) is linearised:

$$A_T = (R/g)\ddot{\theta} - \theta \quad (5)$$

Giving an analytic solution of the form:

$$\theta = C_2 e^{\frac{\sqrt{g}}{\sqrt{R}} t} + C_1 e^{-\frac{\sqrt{g}}{\sqrt{R}} t} - A_T \quad (6)$$

where C_1 and C_2 are constants. The positive power on the C_2 exponential term leads to instability. The system is extremely sensitive to the value of the C_2 and thus the initial conditions.

To illustrate this issue consider synthetic data generated from equation (5). Solving using the exact initial conditions provides the true solution. However, introducing a small error to the θ initial condition ε makes the solution unstable. Figure 3 illustrates this ill conditioning when the error is $\varepsilon = 1e^{-18}$. Even recursive approaches over a much shorter period will not work because any error will quickly grow and corrupt the solution.

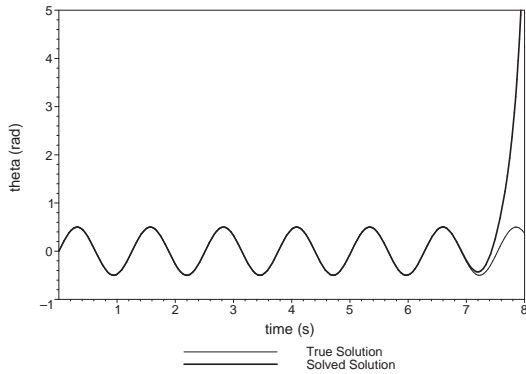


Figure 3: Simulated linearised data, solved analytically using initial conditions with a small error

2.3 Feasible Solution Method

It is clear that this challenging problem requires a novel approach. This section presents a unique solution independent from initial conditions to obtain C_2 with the precision required to give accurate rotational measurement.

Equation (3) is solved over a short period of time. Fitting a cubic function to A_T and A_R over this period effectively filters higher frequency noise:

$$A_{T,fit} = u_1 + u_2 t + u_3 t^2 + u_4 t^3 \quad (7)$$

$$A_{R,fit} = v_1 + v_2 t + v_3 t^2 + v_4 t^3 \quad (8)$$

Substituting equation (7) into equation (3) and making a linear substitution for $\sin(\theta)$ gives:

$$A_{T,fit} = (R/g)\ddot{\theta} - (b_1 + b_2 \theta) \quad (9)$$

where b_1 and b_2 are evaluated by a linear least squares fit to for the past values of θ . A piecewise function improves the fit and allows a longer period to be solved over. However, a separate ODE must be generated and solved for each interval.

Solving equation (9) gives θ_{sol} , the solution for the tangential ODE, defined analytically as:

$$\theta_{sol} = C_2 e^{(mt)} + C_1 e^{(-mt)} + f(t) \quad (10)$$

where C_1 and C_2 are unknown constants and:

$$m = \frac{\sqrt{(b_2 g)}}{\sqrt{R}}$$

$$f(t) = \frac{1}{b_2^2 g} \left(-g b_2 (b_1 + a_1 + a_2 t + a_3 t^2 + a_4 t^3) - 2R(3a_4 t + a_3) \right)$$

If a piecewise substitution for $\sin(\theta)$ is used in equation (9) then all except the first ODE will have initial conditions defined by the previous equation in terms of C_1 and C_2 . Analytical solutions to these subsequent ODEs can be formed, though take up too much space to be shown here. Solving the set of ODEs generates a piecewise solution for θ_{sol} .

Equation (10) is very sensitive to the value of C_2 , as illustrated earlier. The approach taken here is to utilise the independent radial equation (4), to solve for C_1 and C_2 . Substituting θ_{sol} into this equation and approximating $\cos(\theta)$ by a least squares fit to a quadratic function over the whole period gives:

$$A_{R,sol} = (R/g)\dot{\theta}_{sol}^2 - (c_1 + c_2 \theta_{sol} + c_3 \theta_{sol}^2) \quad (11)$$

To find the optimal C_1 and C_2 values a least squares approach fits $A_{R,sol}$ to the radial acceleration, equation (8), over the period. Two independent equations are required which are obtained by differentiating with respect to each constant.

$$Eq_A = \frac{d}{dC_1} \left(\sum_{i=1}^p (A_{R,sol}(t-i) - A_{R,fit}(t-i))^2 \right) \quad (12)$$

$$Eq_B = \frac{d}{dC_2} \left(\sum_{i=1}^p (A_{R,sol}(t-i) - A_{R,fit}(t-i))^2 \right) \quad (13)$$

where p is the number of data points in the period solved over.

Simultaneously solving equations (12) and (13), provides nine pairs of solutions. The real pair that minimises the following equation are selected.

$$Eq_C = \left(\sum_{i=1}^p (A_{R,sol}(t-i) - A_{R,fit}(t-i))^2 \right)^{1/2} \quad (14)$$

The selected C_1 and C_2 are substituted into equation (10) to give orientation for the current time step. The vector containing the past orientation, θ_{old} can then be updated ensuring an accurate fit is achieved for the trigonometric substitutions in equations (9) and (11) for the next time step. Figure 4 summarises this method in a flow-chart.

2.4 Analysis and Performance Metrics

The method is validated using both experimental and synthetic data. Due to the symmetric nature of head motion [15], it is reasonable to use a modified sine wave as basic representative head motion. Allowing the algorithm to be easily tested with different dynamics and noise. The main goals include:

- Verify the model using experimental data from an inverted pendulum.
- An analysis to determine the robustness to noise using synthetic data.
- Determine the dynamic performance of the method.
- Test the method with experimental data.

To measure and quantify performance, the mean absolute error and percentage this is of the mean amplitude of the signal are calculated. For the synthetic data, error is defined as the difference between the solution and θ used to generate the acceleration signals. For the experimental data the error is the difference between the solution and the optical encoder measurement. Standard deviation and maximum error will measure the spread of the fit. These performance metrics are calculated after any initial transient behaviour in the solution has died away.

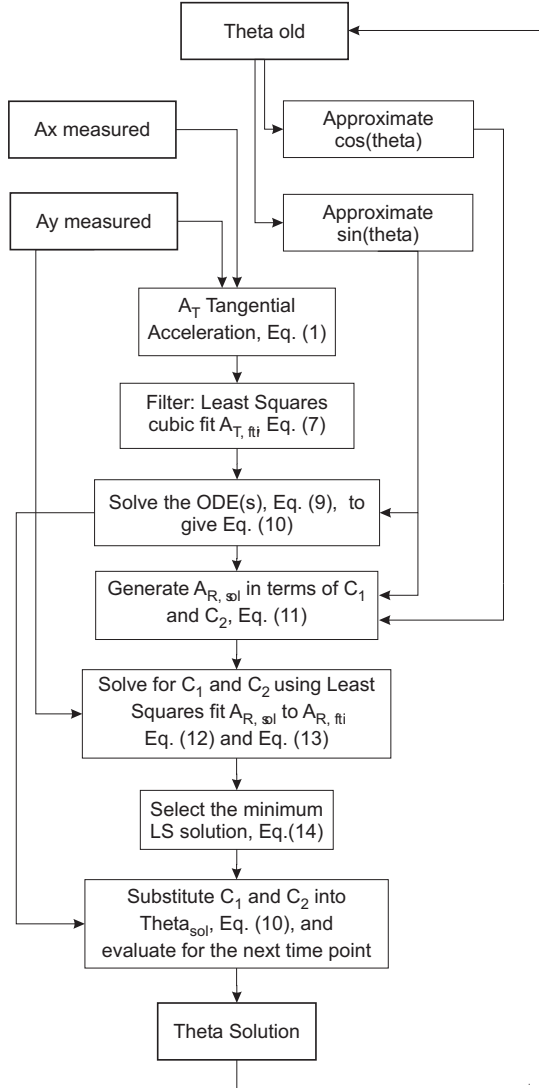


Figure 4: Flow-chart for the solution of θ

3 RESULTS AND DISCUSSION

3.1 Model Verification

To verify that equations (3) and (4) fit the model of the inverted pendulum a simple experiment was conducted. An existing inverted pendulum apparatus was used with an optical encoder providing an independent measure of rotation, θ_{en} . An Analogue Devices ADXL213 dual axis accelerometer was attached to the pendulum at radius $R = 0.3\text{m}$, and at an angle $\lambda = 43.4^\circ$. Data was collected while manually oscillating the pendulum at a slow frequency.

Estimates of the true A_R and A_T were generated using θ_{en} and the model equations (3) and (4). To combat the buildup of noise due to the differentiation of θ_{en} , this signal was filtered to smooth the steps caused by the finite resolution of the encoder. The measured accelerations A_x and A_y were resolved along the tangential and radial axes using equations (1) and (2). A comparison of the model acceleration with the measured accelerations is shown in figure 5.

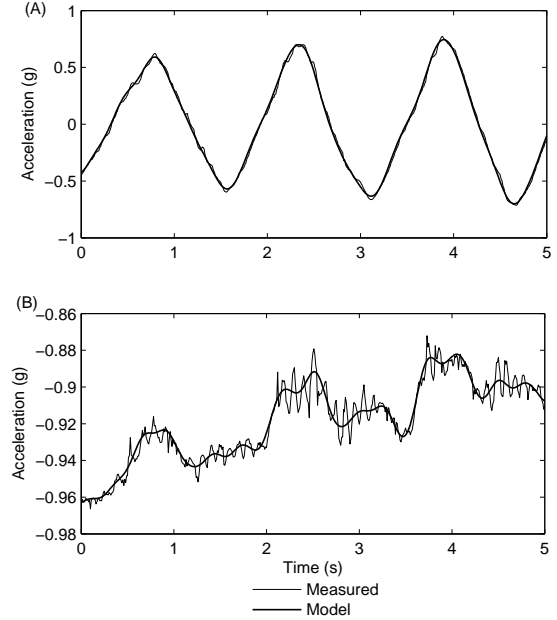


Figure 5: Measured and model tangential (A) and radial (B) acceleration

The mean, standard deviation (STD) and percentage errors are summarised in table 1. A percentage error of 5.4% relative to the mean amplitude shows a good fit between the measured tangential acceleration and the model. However, 21.9% shows the error is much worse for the radial acceleration due to poor sensitivity to orientation when this axis is near vertical.

To determine the accuracy of the model fit to the experimental data in terms of θ , independently from the solution method and noise, equation (3) is integrated giving:

$$\theta = \frac{g}{R} \int_0^t \int_0^t A_T + \frac{g}{R} \int_0^t \int_0^t \sin(\theta) + t\dot{\theta}(0) + \theta(0), \quad (15)$$

Fitting equation (15) to the experimental data

determines the optimal initial conditions $\dot{\theta}(0)$ and $\theta(0)$. This method could also be used to find an optimal R value for later calibration procedures, but here the measured R is used. Evaluating the fit allows an estimate of the model error in terms of theta to be calculated.

The model error is evaluated for each subsequent 0.3s second period. This is the same period that algorithm presented is solved over for each iteration. The final column in table 1 shows the maximum mean error for any section. This error is much less than 1° or 1.1% of the mean signal amplitude in a highly dynamic situation and verifies that the inverted pendulum model does capture the main dynamics for this situation. Explanations for the remaining model error include:

- Missing dynamics due to finite encoder precision.
- Errors in the initial set up, placement of the accelerometer, and zero position of the pendulum.
- Out of plane disturbances affecting the accelerometers.

Table 1: Angular and acceleration model error

Error Measure	Acceleration		Angular θ (deg)
	A_R (mg)	A_T (mg)	
Mean	3.8	20.1	0.17
STD	3.4	13.7	0.04
Percentage	21.9	5.4	1.1

3.2 Robustness to Noise

Noise on the acceleration signals which drive the solutions to the ODE are comprised of two sources. First, the high frequency raw noise from the accelerometer and circuitry. Second, a lower frequency model error that may include motion not captured by the encoder. The method developed is tested using synthetic data at three noise levels and two different linearisation approaches for $\sin(\theta)$ in equation (9).

The noise applied to the synthetic acceleration signals was derived from the mean percentage error in table 1. A single interval of 0.1s was used in the linearisation in Method (A) and a three section piecewise function over 0.3s in Method (B). Results are shown in table 2 and figure 6. A static calculation of rotation is included in the figure for comparison. This simple approach assumes that the change in tangential acceleration is due only to the gravitational component. Thus, taking the inverse sine of A_T yields θ_{simple} .

Table 2: Error response to the presence of noise

Noise	Max (deg)	STD (deg)	Mean (deg)	%
(A) None	0.14	0.01	0.001	0.02
Mean	2.0	0.39	0.42	6.8
2×Mean	2.9	0.56	0.63	10.0
(B) None	0.17	0.02	0.005	0.08
Mean	1.1	0.19	0.17	2.8
2×Mean	1.6	0.28	0.30	4.7

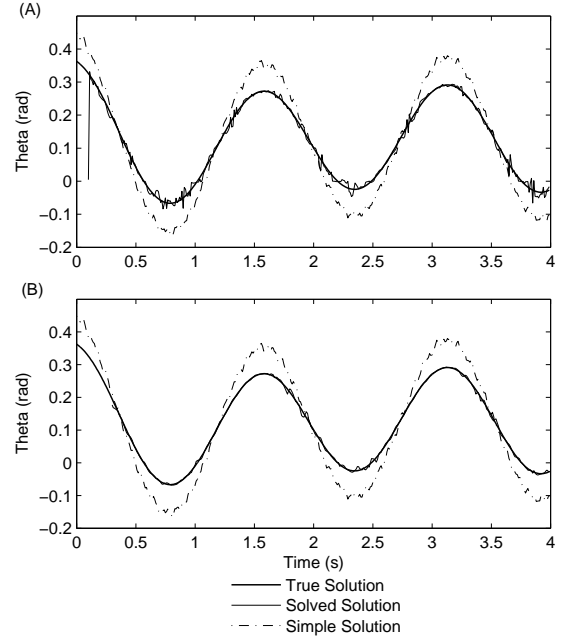


Figure 6: Results for simulated data with mean noise applied solved using Method (A) and Method (B)

Both methods produce results where the mean error is less than 1° . However, Method (B) shows superior performance with approximately half the error and reduced spread in results. For the case where mean noise is applied the maximum error is just over 1° . Solving over a longer period captures more dynamics increasing the amount of signal relative to the noise present. This improves the nine solutions for C_1 and C_2 and reduces the uncertainty in selecting the correct pair in equation (14).

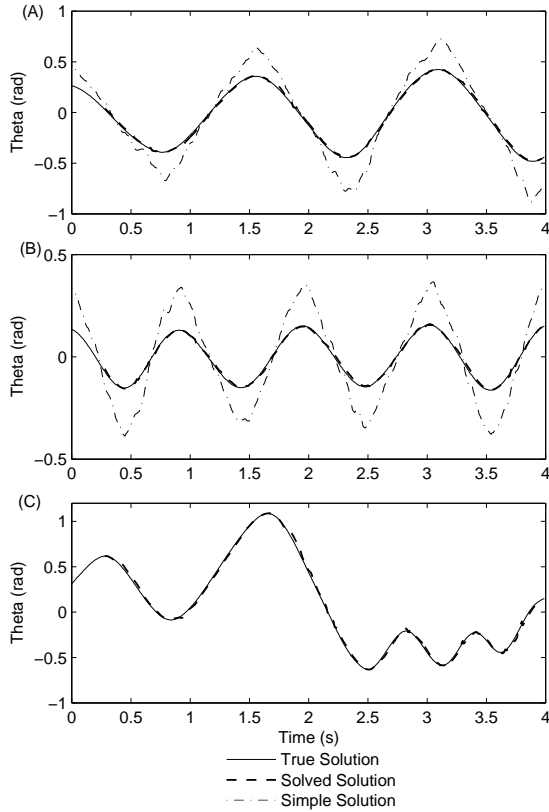
Further improvements can be achieved by optimising the accelerometer placement. Aligning A_R with gravity gives poor sensitivity to static rotations along this axis. This is illustrated in figure 5 with the measured A_R having a very small amplitude and a huge mean error of 21.9%. The radial equation is not solved, it is used to determine the constants C_1 and C_2 in the solution of the tangential equation using a least squares fit. Though, this method is robust in terms of the noise on A_R , improving the signal amplitude increases the accuracy in the final result. Although not practical for all situations, this is achieved by shifting the accelerometer so that it is not directly above the centre of rotation. Hence, separating the vertical and radial axis.

3.3 Experimental Results

Three experiments using the inverted pendulum apparatus were conducted. Different frequency and amplitudes were used to cover a wide range of potential head motion. The acceleration data collected was post-processed using the algorithm with method B to solve for rotation. A comparison of this solution to the reference encoder signal is shown in figure 7 and error metrics in table 3.

Table 3: Experimental error results

Data	Max (deg)	STD (deg)	Mean (deg)	%
A ($\approx 0.75\text{Hz}$)	1.7	0.40	0.61	4.25
B ($\approx 1\text{Hz}$)	0.91	0.23	0.27	5.23
C (random)	3.5	0.65	0.92	—

**Figure 7:** Experimental results for (A), (B), and (C) data sets compared to θ_{en}

4 CONCLUSIONS

Viewpoint tracking methods for augmented reality applications that use HMDs generally suffer from poor dynamic performance. This work achieves dynamic orientation tracking for a single degree of rotation in the vertical plane using only a dual axis accelerometer. Head motion is modelled by that of an inverted pendulum, however instability in the model results in ill conditioning and can not be solved using conventional methods. A unique approach that is independent of initial conditions is presented and evaluated with synthetic and experimental data.

The algorithm presented produces good results with mean error better than 1° for synthetic and experimental data. The integrity of this result is maintained as the dynamics are increased and it does not suffer from drift. The accuracy of the solution is limited by the model error and noise. Latency introduced by this solving method has not been considered. This work proves the initial concept of using an accelerometer to measure dynamic head rotation in a vertical plane.

5 References

- [1] G. Welch and E. Foxlin, "Motion Tracking: No Silver Bullet, but a Respectable Arsenal", *IEEE Computer Graphics and Applications*, 22(6), pp 24–38 (2002).
- [2] G. W. Roberts, A. Evans, A. Dodson, B. Denby, S. Cooper and R. Hollands, "The use of augmented reality, GPS, and INS for subsurface data visualization.", in *FIG XXII International Congress*, Washington, D.C (2002).
- [3] S. You, U. Neumann and R. Azuma, "Orientation Tracking for Outdoor Augmented Reality Registration", *IEEE Computer Graphics and Applications*, 19(6), pp 36–42 (1999).
- [4] E. Foxlin and L. Naimark, "VIS-Tracker: A Wearable Vision-Inertial Self-Tracker", in *VR*, pp 199–206, IEEE Computer Society (2003).
- [5] R. L. Holloway, "Registration Error Analysis for Augmented Reality", *Presence: Teleoperators and Virtual Environments*, 6(4), pp 413–432 (1997).
- [6] E. Foxlin, M. Harrington and Y. Altshuler, "Miniature 6-DOF inertial system for tracking HMDs", in *Proceedings of the SPIE*, volume 3362, pp 214–228, Orlando, FL (1998).
- [7] H. Luinge, P. Veltink and C. Baten, "Estimation of orientation with gyroscopes and accelerometers", in *BMES/EMBS Conference, 1999. Proceedings of the First Joint*, volume 2, p. 844 (1999).
- [8] Inetersense Inc, "Home Page", <http://www.isense.com/>, visited on 1/8/ 2007.
- [9] Ascension Technology Corporation, "Home Page", <http://www.ascension-tech.com/>, visited on 1/8/ 2007.
- [10] Xsens Technology, "Home Page", <http://www.xsens.com/>, visited on 1/8/ 2007.
- [11] Micro Strain, "Home Page", <http://www.microstrain.com/>, visited on 1/8/ 2007.
- [12] R. Azuma and G. Bishop, "A frequency-domain analysis of head-motion prediction", in *SIGGRAPH*, pp 401–408 (1995).
- [13] E. Kraft, "A Quaternion-based Unscented Kalman Filter for Orientation Tracking", in *Proceedings of the 6th Int. Conf. on Information Fusion*, Cairns, Australia (2003).
- [14] L. Chai, K. Nguyen, B. Hoff and T. Vincent, "An Adaptive Estimator for Registration in Augmented Reality", in *Proceedings of IEEE International Workshop on Augmented Reality*, pp 23–32 (1999).
- [15] C. Shaw and J. Liang, "An experiment to characterize head motion in VR and RR using MR", in *Proceedings of the 1992 Western Computer Graphics Symposium*, pp 99–101 (1992).